Steel and Composite Structures, *Vol. 28, No. 5 (2018) 589-606*
DOI: https://doi.org/10.12989/scs.2018.28.5.589

Exact vibration and buckling analyses of arbitrary gradation of nano-higher order rectangular beam

Abbas Heydari*

Young Researchers and Elite Club, Ardabil Branch, Islamic Azad University, Ardabil, Iran

(*Received December 1, 2017, Revised May 3, 2018, Accepted June 23, 2018*)

Abstract. The previous studies reflected the significant effect of neutral-axis position and coupling of in-plane and out-of-plane displacements on behavior of functionally graded (FG) nanobeams. In thin FG beam, this coupling can be eliminated by a proper choice of the reference axis. In shear deformable FG nanobeam, not only this coupling can't be eliminated but also the position of neutral-axis is dependent on through-thickness distribution of shear strain. For the first time, in this paper it is avoided to guess a shear strain shape function and the exact shape function and consequently the exact position of neutral axis for arbitrary gradation of higher order nanobeam are obtained. This paper presents new methodology based on differential transform and collocation methods to solve coupled partial differential equations of motion without any simplifications. Using exact position of neutral axis and higher order beam kinematics as well as satisfying equilibrium equations and traction-free conditions without shear correction factor requirement yields to better results in comparison to the previously published results in literature. The classical rule of mixture and Mori-Tanaka homogenization scheme are considered. The Eringen's nonlocal continuum theory is applied to capture the small scale effects. For the first time, the dependency of exact position of neutral axis on length to thickness ratio is investigated. The effects of small scale, length to thickness ratio, Poisson's ratio, inhomogeneity of materials and various end conditions on vibration and buckling of local and nonlocal FG beams are investigated. Moreover, the effect of axial load on natural frequencies of the first modes is examined. After degeneration of the governing equations, the exact new formulas for homogeneous nanobeams are computed.

Keywords: free vibration; buckling; arbitrary functionally graded beam; nonlocal elasticity theory; exact shear strain shape function

1. Introduction

Neglecting the shear stress in Euler-Bernoulli beam theory or assuming a constant shear stress in Timoshenko beam model, however simplifies the solutions of beam problems but yields to an unreal estimating of beam's behavior. Using higher order beam kinematics and satisfying the traction-free conditions at free surfaces of the beam, develops the simplified kinematics of the Euler-Bernoulli and Timoshenko beam models. The various higher order shear deformation beam models are proposed by many researchers to approximate the behavior of shear deformable nano and macro beams. The Timoshenko beam model is developed due to approximate the axial displacement by higher order polynomials (Reddy 1984, Shi 2007, Thai and Vo 2012b). The model of Touratier includes a sinusoidal approximation of shear stress (Touratier 1991). Some researchers used an exponential variation for approximating shear stress distribution (Karama *et al*. 2003). Also the distribution of shear stress in model of Mechab is expressed in terms of hyperbolic functions (Mechab 2009). For the bending analysis of simply supported FG shell, the optimized sinusoidal higher order shear deformation theory is proposed (Mantari and Guedes Soares 2014). A higher order shear and normal deformation theory including five unknown functions using approximated hyperbolic displacement field is applied to analyze bending and free vibration of FG plates (Belabed *et al*. 2014). A through-thickness sinusoidal variation for approximating displacement field is proposed to study elastic deformation of shear deformable thick FG plates having variable stiffness through their length (Amirpour *et al*. 2016). A sinusoidal shear deformation theory is proposed to approximate the bending, buckling and vibration behavior of homogeneous nonlocal beams (Thai and Vo 2012b). The higher order transversely functionally graded beam theories for approximating static bending and vibration behavior of micro-beams (Şimşek and Reddy 2013) and macro structure beams using parabolic shear deformation (Hadji *et al*. 2016) are proposed. A new higher order shear deformation theory for estimating vibration and stability responses of FG sandwich plate is proposed by Sekkal *et al*. (2017). A new four variable refined plate theory for estimating buckling behavior of FG plates is proposed by Bellifa *et al*. (2017). A novel higher order shear deformation theory (HSDT) is proposed for estimating buckling behavior of FG sandwich plates subjected to thermal loading (Menasria *et al*. 2017). The Eringen's nonlocal elasticity theory and strain gradient elasticity

*Corresponding author, Ph.D.,
E-mail: a_heydari@alum.sharif.edu;
a_heydari@tabrizu.ac.ir

ISSN: 1229-9367 (Print), 1598-6233 (Online)

model are applied to the higher order shear beam models and other beam mechanics like the Euler-Bernoulli and Timoshenko beam theories to predict vibration and buckling behavior of simply supported composite micro and nano beams (Challamel 2013). Challamel show that Shi–Voyiadjis and Bickford–Reddy higher order shear beam models have the kinematics equivalence, especially in vibration and buckling behaviors. Also the mentioned research show that the higher order shear beam models are classified in a traditional gradient elasticity Timoshenko beam theory. Meanwhile, for the case of dynamic analyses the nonlocal beam model is equivalent to higher order inertia beam model. In contrast to the above-mentioned and many other similar researches, the present work aims to find an exact through-thickness distribution of shear strain and avoids guessing a shape function for across-the-thickness variation of shear strain. Therefore for the first time, the exact position of neutral axis for free vibration and buckling analyses of higher order FG local and nonlocal beams is considered. The size effect phenomena on behavior of nanostructures are explained by the differential or integral form of the nonlocal continuum theory. Eringen's nonlocal theory has been proposed for the non-neighbor interactions between the building units of the material microstructure (Eringen 1972a, b, 1978, Eringen and Edelen 1972, Eringen and Kim 1974, Eringen *et al*. 1977). Eringen's integral nonlocal theory incorporates an integral operator to sum the nonlocal residuals inside the material (Eringen and Kim 1974, Eringen *et al*. 1977, Eringen 1978). In 1983, the integral operator was replaced by a differential operator introducing the differential nonlocal theory (Eringen 1983). Nonlocal theories for nanobeams and nanotubes are applied (Reddy 2007, Reddy and Pang 2008). Reddy (2010) reformulated the conventional governing equations of shear deformable beam and plates using nonlinear strains and Eringen's nonlocal continuum theory. Rahmani and Pedram (2014) discussed the vibration of FGBs based on Timoshenko beam and Eringen nonlocal elasticity theories. The Finite Element approach using continuum mechanics and nonlocal thermodynamics is applied to analyze bending behavior of homogeneous nanobeams (de Sciarra 2013). The Hamilton's principle, Timoshenko and nonlocal beam theories and Maxwell equation are used to investigate free vibration, buckling and bending of magneto-electro-elastic nanobeams (Li *et al*. 2015). Flexural vibration and buckling analysis of single-walled carbon nanotubes using different gradient elasticity theories based on Reddy and Huu-Tai formulations is conducted by Karličić *et al*. (2015). Nonlocal forced vibration of a double single-walled carbon nanotube system under the influence of an axial magnetic field is studied by Stamenković *et al*. (2016). Mode shape and vibration analysis of sandwich panel with multiwalled carbon nanotubes (MWCNTs) FG-reinforcement core is studied by Tahouneh (2017). The free vibration and buckling analyses of tapered FG thin beam-column having general natural end conditions is investigated (Rezaiee-Pajand and Masoodi 2017). Buckling and postbuckling behavior of nanotubes are investigated by She *et al*. (2017). Nonlinear vibration of multi-body systems with linear and nonlinear springs is presented by Bayat *et al*. (2017). Vibration of a rotary FG plate with consideration of thermal and Coriolis effects is studied by Ghadiri *et al*. (2017). Vibration analysis of FG nanobeams based on third-order shear deformation theory for simple power law distribution is done by Jandaghian and Rahmani (2017). The Gurtin-Murdoch model is based on a hybrid formulation combining linearized deformation of bulk material with second-order finite deformation of the surface. The equations of the linearized Gurtin-Murdoch model of surface elasticity can be derived from the ratio of deformed surface area to initial surface area (Ru 2010). Oskouie and Ansari (2017) used the fractional calculus to analyze the vibrations of viscoelastic Timoshenko nanobeams. They used the Gurtin–Murdoch surface stress theory to consider the surface effects. They applied two numerical and semi-analytical solution procedures including the generalized differential quadrature and finite difference methods for linear and the Galerkin approach and predictor–corrector method for nonlinear partial differential governing equations. The Mori-Tanaka method (Mori and Tanaka 1973) was originally concerned with calculating the average internal stress in matrix of a material containing precipitates with eigenstrains. Bending and vibration of functionally graded higher order microbeams by using Mori-Tanaka technique and the modified couple stress theory are studied (Şimşek and Reddy 2013). The surface stress, surface density and surface elasticity effects on nonlinear free vibration of nonlocal thin functionally graded beams are considered by Hosseini-Hashemi *et al*. (2014). The sixth-order finite difference discretization is used to discretize the governing equation of motion and boundary conditions of nonlocal thin beam rested on two-parameter elastic foundation by Mohamed *et al*. (2016). The stability and free vibration analyses of a simply supported Euler–Bernoulli multiple-nanobeam system under the influence of axial load using the Eringen nonlocal continuum theory is conducted by Karličić *et al*. (2016). They used D'Alembert's principle to obtain the partial differential equations of motion of the system. Also, the classical Bernoulli–Fourier method and trigonometric method are used to obtain analytical solutions. A normalized symmetric kernel is employed to analyze the nonlocal integral elasticity of beams by Koutsoumaris *et al*. (2017). Rise to paradoxes and energy inconsistent formulas in the nonlocal integral forms are vanished. The vibration of nano-beam surrounded by two-parameter Pasternak foundation type in thermal environments is studied by Demir and Civalek (2017). They used variational approach and Hamilton's principle to obtain the nonlocal Euler–Bernoulli governing equations of motion. The Hermitian cubic shape functions and Galerkin method of weighted residuals are used to calculate the mass and stiffness matrices. He *et al*. (2016) proposed a new higher order two-layer composite beam model having partial interaction finer than the Reddy's higher order beam theory. In their research, the Reddy's theory is modified and the Laplace transform technique is applied to find the axial forces and natural frequencies. The differential transform method (DTM) is introduced by Zhou (1986). This method is a semi-numerical-analytic scheme without linearization or perturbation requirements which leads to a closed form or an approximate solution. In contrast to the traditional high order Taylor's series method, which requires large computational work for large orders, the DTM leads to highly accurate results in less time without round-off errors. The DTM transforms the given ordinary or partial differential equation and related boundary or initial conditions into a recurrence equation. A wide variety of problems including the differential difference equations, fractional differential equations, pantograph equations, integro-differential equations and matrix differential equations are solved by DTM (Arikoglu and Ozkol 2005, 2006, 2007, Abazari 2009, Keskin *et al*. 2007). The collocation method is applied on a finite-dimensional space of candidate solution and the boundary conditions are met. The collocation method is used for solving static and dynamic beam problems, multi-term fractional partial differential equations and multidimensional wave type equations (Ren and Tian 2016, Wattanasakulpong and Mao 2015, Reutskiy 2017, Bhrawy *et al*. 2015). Heydari et al. (2017) employed collocation and spectral Ritz methods to analyze stability of thin and thick FG circular plates having linear and quadratic thickness variations rested on two-parameter elastic medium. For some problems, analyses of structures made up of FGM have been done (Heydari 2013, 2015, Heydari and Shariati 2018). ANFIS is applicable for analytical modeling of FG beam (Toghroli *et al*. 2018). This paper presents new methodology to solve free vibration and stability problems of nanostructure higher order shear deformable rectangular FG nanobeams having arbitrary material gradation by considering coupled partial differential equations of motion without any simplifications. Using higher order beam kinematics, satisfying equilibrium equations and shear stress-free conditions at top and bottom surfaces of the beam's section yields to accurate solutions due to compute the exact shear strain distribution and therefore the exact position of neutral axis. The natural circular frequencies and buckling loads of the first modes are obtained by considering small scale effects and shear deformation without shear correction factor requirement by using differential transformation and collocation methods. For the first time, the dependency of exact position of neutral axis on length to thickness ratio in higher order shear deformable FG nanobeam is investigated. The Eringen's nonlocal continuum theory is applied to capture the small scale effects. Two homogenization schemes, the classical rule of mixture and Mori-Tanaka technique are used to model the through-thickness variations of mass and mechanical properties. The various classical end conditions for buckling analysis and pinned boundary condition for vibration analysis are considered. In our model, increasing the length to thickness ratio yields to change the through-thickness distribution of axial strain from nonlinear distribution for thick FGB to a linear distribution for thin FGB. Also, for thin FGB the shear strain is vanished. The maximum shear stress is occurred at neutral axis which is located at top of the mid-axis. The analytical formulas in the case of the homogeneous beams are obtained. The results of present study are more accurate than the previously published results in literature due to considering the exact position of neutral axis for higher order shear deformable FG nanobeam.

2. Higher order transversely functionally graded beam

A rectangular functionally graded beam (FGB) having arbitrary through-thickness material gradation with the axial displacement $u(x,y)$ and deflection $w(x)$ is assumed. The right-handed coordinate system (x,y) is considered, in which x axis is located along the axis of the beam and y axis is upside positive. The origin of y ordinate is selected based on the reference axis which is used for mathematical definition of the mass density and elastic modulus. The distance between origin of y and top and bottom fibers of the beam are c_t and c_b respectively. The neutral axis is located at somewhere rather than the position of reference axis. The parameter $\bar{y}$ denotes the distance between neutral axis and reference axis. The above-mentioned parameters and geometry of FGB are demonstrated in Fig. 1.

2.1 Buckling analysis of FGB for various boundary conditions

The components of engineering strain tensor are considered as follows

$$\begin{aligned} \varepsilon_{xx} &= u_{,x} \\ \varepsilon_{xy} &= \frac{1}{2}\left(u_{,y} + w_{,x}\right) \\ \varepsilon_{yy} &= 0 \end{aligned} \tag{1}$$

where subscripts $,x$ and $,y$ denote partial derivatives with respect to x and y respectively. The shear strain is assumed as follows

$$\gamma_{xy} = f_{,y} \tag{2}$$

in which $\gamma_{xy} = 2\varepsilon_{xy}$ is shear strain and f is an unknown function in terms of x and y to be determined. Substituting ε_{xy} from Eq. (2) into Eq. (1) and integrating from the resultant with respect to y, one has

$$u = f - w_{,x}y + u_0 \tag{3}$$

The function u_0 is an unknown function in terms of x

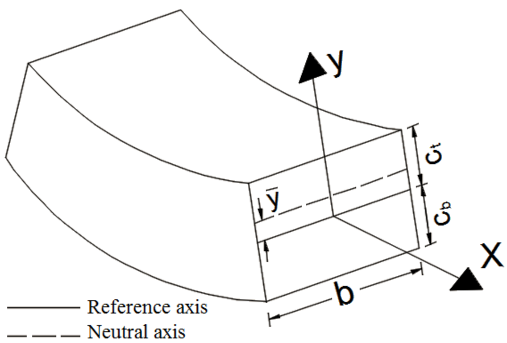

Fig. 1 The cross section of FGB

that arising from the integration. The function u_0 is the axial displacement at origin of y ordinate. Substituting Eq. (3) into Eq. (1) after considering Hooke's law, yields

$$\begin{gathered}\sigma_{xx} = E\left(f_{,x} - w_{,xx}y + u_{0,x}\right)\\ \tau_{xy} = Gf_{,y}\\ G = \frac{E}{2(1+\nu)}\end{gathered} \tag{4}$$

in which σ_{xx}, τ_{xy}, E, G and ν are axial stress, shear stress, modulus of elasticity, shear modulus and Poisson's ratio respectively. The modulus of elasticity and shear modulus are arbitrary functions in terms of y. In the beam subjected to pure bending the sum of all infinitesimal axial forces must be vanished. Therefore the integration of axial stress over the cross section is set equal to zero.

$$\int_{-c_b}^{c_t} bEf_{,x}\,dy - I_2 w_{,xx} + I_1 u_{0,x} = 0 \tag{5}$$

in which the parameter b is width of the section. The constants I_1 and I_2 are as follows

$$I_1 = \int_{-c_b}^{c_t} bEdy, \qquad I_2 = \int_{-c_b}^{c_t} bEydy \tag{6}$$

After integrating from Eq. (5) with respect to x, the axial displacement at origin of y is obtained as follows

$$u_0 = \frac{I_2}{I_1}w_{,x} - \frac{1}{I_1}\int\int_{-c_b}^{c_t} bEf_{,x}\,dydx \tag{7}$$

The shear stress resultant is calculated by integrating the shear stress in Eq. (4) over the cross section, A. It is noteworthy to mention that the change of shear stress resultant in longitudinal direction of FGB is equal to the change of shear force which is imposed to the beam due to axial compression, P.

$$\frac{\partial}{\partial x}\int Gf_{,y}\,dA = Pw_{,xx} \tag{8}$$

The function f is determined after considering this fact that the resultant of integration in left-hand side of Eq. (8) must be equal to the product of a constant to curvature of FGB, $w_{,xx}$.

$$f = \varphi w_{,x} \tag{9}$$

where φ is an unknown function in terms of y to be determined. Considering Eqs. (8)-(9), yields to obtain the buckling load of higher order shear deformable rectangular FGB having arbitrary gradation of elasticity modulus as follows

$$P = \frac{1}{2(1+\nu)}\int_{-c_b}^{c_t} bE\varphi_{,y}\,dy \tag{10}$$

The function φ can be determined by considering the equilibrium equation in x direction.

$$\frac{\partial}{\partial x}\sigma_{xx} + \frac{\partial}{\partial y}\tau_{xy} = 0 \tag{11}$$

Substituting Eqs. (7)-(9) in Eqs. (4) and substituting the resultant into Eq. (11), yields

$$\begin{gathered}2(1+\nu)\left(\varphi - y + \frac{I_2}{I_1} - \frac{I_3}{I_1}\right)w_{,xxx}\\ +\left(\frac{E_{,y}}{E}\varphi_{,y} + \varphi_{,yy}\right)w_{,x} = 0\end{gathered} \tag{12}$$

in which the constant I_3 is defined in Eq. (13).

$$I_3 = \int_{-c_b}^{c_t} bE\varphi\,dy \tag{13}$$

All terms of Eq. (12) rather than $w_{,x}$ and $w_{,xxx}$ are functions of y. Therefore one can write $w_{,xxx} = -\beta w_{,x}$, where β is a numeric constant. After differentiating from $w_{,xxx} + \beta w_{,x} = 0$ with respect to x, and solving the resultant ODE, one has

$$w = c_0 + c_1 x + c_2 \sin(\sqrt{\beta}\,x) + c_3\cos(\sqrt{\beta}\,x) \tag{14}$$

The Eq. (14) is the deflection of buckled Euler-Bernoulli FGB. Therefore the constant β is equal to the P_E/EI, in which EI and P_E are the bending rigidity and buckling load of Euler-Bernoulli FGB respectively. In general, β is equal to $N\pi^2/L^2$, in which L is length of the beam and the values of dimensionless parameter N for simply supported (S-S), clamped (C-C), simply clamped (S-C) and cantilever (C-F) end conditions are calculated according to the Euler-Bernoulli beam theory (Table 1).

The Eq. (12) is rewritten by considering $w_{,xxx} = -\beta w_{,x}$ as follows

$$\varphi_{,yy} + \frac{E_{,y}}{E}\varphi_{,y} - 2\beta(1+\nu)\left(\varphi - y + \frac{I_2}{I_1} - \frac{I_3}{I_1}\right) = 0 \tag{15}$$

The parameter I_3 is depended on unknown function φ. For neglecting the unknown parameter I_3, the derivative of Eq. (15) with respect to y is calculated. The function ϕ is equal to $\varphi_{,y}$.

$$\begin{gathered}\phi_{,yy} + \frac{E_{,y}}{E}\phi_{,y} + \left(\frac{E_{,yy}}{E} - \left(\frac{E_{,y}}{E}\right)^2\right)\phi\\ -2\beta(1+\nu)(\phi - 1) = 0\end{gathered} \tag{16}$$

Table 1 The values of N for first five modes and various boundary conditions

End condition	Mode number				
	1	2	3	4	5
S-S	1.000000	4.000000	9.000000	16.000000	25.000000
C-C	4.000000	8.182994	16.000000	24.187197	36.000000
S-C	2.045749	6.046799	12.047075	20.047188	30.047244
C-F	0.250000	2.250000	6.250000	12.250000	20.250000

The traction-free condition for shear stress at top and bottom surfaces of FGB implies that ϕ at $y = c_t$ and $y = -c_b$ must be vanished. Therefore there is no need to use the shear correction factor in Eq. (10) to calculate the buckling load of higher order FGB.

2.2 Vibration analysis of pinned FGB subjected to axial load

It is possible to obtain a complete solution through separation of variables of partial differential equation of motion. Assuming deflection function as product of two independent functions $w(x)$ and $\exp(I\omega t)$, and considering equilibrium equation in transverse direction, yields

$$\frac{\partial}{\partial x}\int \tau_{xy}\, dA - P w_{,xx} = -m_0 \omega^2 w \tag{17}$$

where

$$m_0 = \int_A \rho dA \tag{18}$$

The parameter ω is circular frequency of vibration. The sign of axial compression, P, is taken to be positive. It is assumed that f in Eq. (2) is a separable two variable function as follows

$$f = \psi \int w dx \tag{19}$$

where ψ is an unknown function in terms of y and ω to be determined. The axial displacement after considering the Eqs. (3) and (19) is calculated in Eq. (20). The numerical results indicate that in contrast to the homogeneous beam the function ψ at origin (y = 0) of FGB is nonzero, therefore u in Eq. (20) at origin is nonzero. In addition, after neglecting u_0 the convergence of fundamental natural frequency is observed and verified by the outcomes of the previous works.

$$u = \psi \int w dx - w_{,x} y \tag{20}$$

The stress field of FGB by considering Eqs. (4) and (19) is obtained as follows

$$\begin{gathered} \sigma_{xx} = E\left(\psi w - w_{,xx} y\right) \\ \tau_{xy} = G\psi_{,y} \int w dx \end{gathered} \tag{21}$$

The equilibrium equation of FGB in longitudinal direction, can be written as follows

$$\frac{\partial}{\partial x}\sigma_{xx} + \frac{\partial}{\partial y}\tau_{xy} = \rho \ddot{u} \tag{22}$$

where $\ddot{u}$ is axial acceleration and takes the value $-u\omega^2$. Substituting Eq. (20) and Eqs. (21) into Eq. (22), one has

$$\begin{gathered} E\left(\psi w_{,x} - w_{,xxx} y\right) + G_{,y}\psi_{,y} \int w dx + G\psi_{,yy} \int w dx \\ +\rho\omega^2 \left(\psi \int w dx - y w_{,x}\right) = 0 \end{gathered} \tag{23}$$

For simply supported FGB, the sinusoidal deflection function is assumed as follows

$$w = \sin\left(\frac{\bar{m}\pi x}{L}\right) \tag{24}$$

where $\bar{m}$ denotes the number of mode. After substituting Eq. (24) into Eq. (23), the Eq. (25) is obtained.

$$\begin{gathered} G L^4 \psi_{,yy} + G_{,y} L^4 \psi_{,y} + (\rho\omega^2 L^2 - \bar{m}^2\pi^2 E) \\ (L^2\psi + \bar{m}^2\pi^2 y) = 0 \end{gathered} \tag{25}$$

The shear stress-free condition at top and bottom surfaces of FGB implies that $\psi_{,y}$ at $y = c_t$ and $y = -c_b$ must be vanished. After using numerical methods and satisfying boundary conditions, the function ψ can be obtained. Considering Eqs. (17) and Eq. (21), yields

$$\left(\int G\psi_{,y}\, dA + m_0\omega^2\right) w - P w_{,xx} = 0 \tag{26}$$

By substituting Eq. (24) into Eq. (26), the Eq. (27) is written. The natural circular frequencies of first modes for simply supported higher order FGB will be obtained after solving the Eq. (27) with respect to ω.

$$\left(\int G\psi_{,y}\, dA + m_0\omega^2\right) L^2 + \bar{m}^2\pi^2 P = 0 \tag{27}$$

3. Solutions of differential equations

The analytical solutions for buckling and free vibration problems of homogeneous beam are provided in Section 3.1. For FGB, the differential transformation method (DTM) and collocation method (CM) are used in Sections 3.2 and 3.3 to obtain the numerical solutions. The DTM and CM are used to have the faster convergence for fractional values and great amounts of material exponent parameter respectively.

3.1 Analytical solutions for homogeneous beam

After degenerating Eq. (16), the governing differential equation for bucking of homogeneous beam is obtained ($E_{,y}$ = $E_{,yy}$ = 0). The function ϕ can be obtained by solving the governing differential equation and satisfying the traction free conditions. The stress field of buckled rectangular higher order homogeneous beam can be obtained from Eqs. (4) as follows

$$\begin{gathered} \sigma_{xx} = -E w_{,xx} \\ \left(\frac{\sinh\left(\sqrt{2\pi^2 N(1+\nu)/L^2}\, y\right)}{\sqrt{2\pi^2 N(1+\nu)/L^2}\cosh\left(\sqrt{\pi^2 N(1+\nu)/2L^2}\, h\right)}\right) \\ \tau_{xy} = G w_{,x}\left(1 - \frac{\cosh\left(\sqrt{2\pi^2 N(1+\nu)/L^2}\, y\right)}{\cosh\left(\sqrt{\pi^2 N(1+\nu)/2L^2}\, h\right)}\right) \end{gathered} \tag{28}$$

where '$\sin h$' and '$\cos h$' are hyperbolic sine and cosine functions. For rectangular homogeneous beam having classical boundary condition, the critical load is obtained from Eq. (10) in terms of hyperbolic tangent function as follows

$$P_{cr}^{H} = GA\left(1 - \frac{\sqrt{2}R\tanh\left(\pi\sqrt{N(1+\nu)/2R^2}\right)}{\pi\sqrt{N(1+\nu)}}\right) \quad (29)$$

where h and R are thickness and length to thickness ratio respectively. The other parameters were introduced in Section 2. By approaching R to zero, P_{cr}^{H} approaches to GA. In addition, by approaching R to infinity, the ratio of P_{cr}^{H} to P_E, approaches to one. For thin beam the parameter R approaches to infinity and the shear stress is vanished. For this case, the axial stress is simplified to the $Ew_{,xx}y$, which is a linear through-thickness variation.

After degenerating Eq. (25), the governing differential equation of motion for vibration of homogeneous beam is obtained (G_y = 0). The function ψ can be obtained by solving the governing differential equation of motion and satisfying the traction free conditions. The stress field caused by free vibration for simply supported rectangular higher order homogeneous beam subjected to axial load is obtained from Eq. (21) as follows

$$\begin{gathered}
\sigma_{xx} = \bar{m}^2\pi^2 E w^{\max}\sin(\bar{m}\pi x/L) \\
\sin h\left(\sqrt{2\bar{m}^2\pi^2(1+\nu)/L^2 - \rho\omega^2/G y}\right)/[\\
L^2\cos h\left(\sqrt{\bar{m}^2\pi^2\,(1+\nu)/2L^2 - \rho\omega^2/4G h}\right) \\
\sqrt{2\bar{m}^2\pi^2(1+\nu)/L^2 - \rho\omega^2/G}] \\
\tau_{xy} = \bar{m}\pi G w^{\max}\cos(\bar{m}\pi x/L)/L[1 - \\
\cos h\left(\sqrt{2\bar{m}^2\pi^2(1+\nu)/L^2 - \rho\omega^2/G y}\right)/ \\
\cos h\left(\sqrt{\bar{m}^2\pi^2(1+\nu)/2L^2 - \rho\omega^2/4G h}\right)]
\end{gathered} \quad (30)$$

where $w^{\max}$ is the maximum deflection of the beam. The vibration characteristic equation of higher order shear deformable rectangular homogeneous beam subjected to axial load is obtained from Eq. (27) as follows

$$\begin{gathered}
2\tan h\left(\sqrt{\bar{m}^2\pi^2(1+\nu)/2L^2 - \rho\omega^2/4G h}\right)/ \\
\left(\sqrt{2\bar{m}^2\pi^2(1+\nu)/L^2 - \rho\omega^2/G h}\right) \\
+\rho\omega^2 L^2/(G\bar{m}^2\pi^2) = 1 - P/GA
\end{gathered} \quad (31)$$

The minimum positive root of the characteristic equation is the frequency of vibration for $\bar{m}^{th}$ mode. The fundamental natural frequency will be obtained for $\bar{m} = 1$.

3.2 Differential transformation method

The differential transformation technique is an iterative procedure which can be used to obtain the sufficiently differentiable answer of an ordinary differential equation. This method generates a recurrence equation and therefore the high-order Taylor series expansion of answer is obtained with the less computational efforts. This method is used to have a faster convergence for fractional values of material exponent parameter. The m-partial sums of Taylor polynomial for function ϕ in Eq. (16) about the origin of y (about the reference axis or mid-axis) is assumed as follows

$$\phi \approx \sum_{k=0}^{m}\Phi(k)y^k \quad (32)$$

The differential transform of coefficients of ODE in Eq. (16) are presented in Eq. (33).

$$\begin{gathered}
C_2(i) = \delta(i) \\
C_1(i) = \frac{1}{i!}\frac{d^i}{(dy)^i}\left(\frac{E_{,y}}{E}\right)\Bigg|_{y=0} \\
C_0(i) = \frac{1}{i!}\frac{d^i}{(dy)^i}\left(\frac{E_{,yy}}{E} - \left(\frac{E_{,y}}{E}\right)^2\right)\Bigg|_{y=0} - 2\beta(1+\nu)\delta(i)
\end{gathered} \quad (33)$$

The differential transform of ODE in Eq. (16) is presented in Eq. (34).

$$\begin{gathered}
\sum_{j=0}^{2}\sum_{i=0}^{k}C_j(i)\frac{(k+j-i)!}{(k-i)!}\Phi(k+j-i) \\
+2\beta(1+\nu)\delta(k) = 0 \\
k \in \{0,1,2,\ldots,m\}
\end{gathered} \quad (34)$$

where

$$\delta(r) = \begin{cases}1 & r = 0\\ 0 & r \neq 0\end{cases} \quad (35)$$

The recurrence equation is obtained by considering Eq. (34) as follows

$$\begin{gathered}
\Phi(k+2) = -\frac{k!}{(k+2)!} \\
\left[\sum_{j=0}^{1}\sum_{i=0}^{k}C_j(i)\frac{(k+j-i)!}{(k-i)!}\Phi(k+j-i)\right. \\
\left. - + 2\beta(1+\nu)\delta(k)\right]
\end{gathered} \quad (36)$$

The Eq. (36) shows that the truncated Taylor series expansion of function ϕ can be written in terms of $\phi(0)$ and $\phi_{,y}(0)$ or $\Phi(0)$ and $\Phi(1)$. The differential transform of traction-free conditions are

$$\begin{gathered}
\sum_{k=0}^{m}\Phi(k)\left(\frac{h}{2}\right)^k = 0 \\
\sum_{k=0}^{m}(-1)^k\Phi(k)\left(\frac{h}{2}\right)^k = 0
\end{gathered} \quad (37)$$

By using Eqs. (37), the unknown coefficients $\Phi(0)$ and $\Phi(1)$ and an approximation of unknown function ϕ about the mid-axis will be obtained. Increasing order of Taylor series expansion in Eq. (32), yields to an accurate solution.

The buckling loads of first modes for higher order shear deformable FGB are obtained by substituting Eq. (32) into Eq. (10) as follows

$$P=\frac{b}{2(1+\nu)}\sum_{k=0}^{m}\Phi(k)\int_{-c_b}^{c_t}Ey^k dy \tag{38}$$

Using similar procedure yields to solve the differential equation of motion of higher order shear deformable FGB. The approximation of the function ψ is shown in Eq. (39).

$$\psi\approx\sum_{k=0}^{m}\Psi(k)y^k \tag{39}$$

where Ψ is the differential transform of ψ. The differential transform of coefficients of ODE in Eq. (25) are presented in Eq. (40)

$$\begin{aligned}\tilde{C}_2(i)&=\frac{L^4}{i!}\frac{d^i}{(dy)^i}(G)\bigg|_{y=0}\\ \tilde{C}_1(i)&=\frac{L^4}{i!}\frac{d^i}{(dy)^i}\left(G_{,y}\right)\bigg|_{y=0}\\ \tilde{C}_0(i)&=\frac{L^2}{i!}\frac{d^i}{(dy)^i}(\rho\omega^2L^2-\bar{m}^2\pi^2E)\bigg|_{y=0}\end{aligned} \tag{40}$$

The differential transform of ODE in Eq. (25) is obtained in Eq. (41).

$$\begin{gathered}\sum_{j=0}^{2}\sum_{i=0}^{k}\tilde{C}_j(i)\frac{(k+j-i)!}{(k-i)!}\Psi(k+j-i)+\bar{m}^2\pi^2\,\tilde{\delta}(k)\\ (\rho\omega^2L^2-\bar{m}^2\pi^2E)=0\quad k\in\{0,1,2,\ldots,m\}\end{gathered} \tag{41}$$

where

$$\tilde{\delta}(r)=\begin{cases}1 & r=1\\ 0 & r\neq 1\end{cases} \tag{42}$$

The recurrence equation by considering Eq. (41) is obtained as follows

$$\begin{aligned}\Psi(k+2)=&-\frac{k!}{G\,|_{y=0}L^4(k+2)!}\\ &\left[\sum_{i=1}^{k}\tilde{C}_2(i)\frac{(k+2-i)!}{(k-i)!}\Psi(k+2-i)+\right.\\ &\sum_{j=0}^{1}\sum_{i=0}^{k}\tilde{C}_j(i)\frac{(k+j-i)!}{(k-i)!}\Psi(k+j-i)\\ &\left.-+(\rho\omega^2L^2-\bar{m}^2\pi^2E)\,\bar{m}^2\pi^2\,\tilde{\delta}(k)\right]\end{aligned} \tag{43}$$

According to the Eq. (43), the truncated Taylor series expansion of function ψ can be written in terms of $\Psi(0)$ and $\Psi(1)$. The differential transform of traction-free conditions are

$$\begin{gathered}\sum_{k=1}^{m}\Psi(k)k\left(\frac{h}{2}\right)^{k-1}=0\\ \sum_{k=1}^{m}(-1)^{k-1}\Psi(k)k\left(\frac{h}{2}\right)^{k-1}=0\end{gathered} \tag{44}$$

Using Eqs. (44) yields to obtain the unknown coefficients $\Phi(0)$ and $\Phi(1)$. Therefore an approximation of unknown function ϕ about the mid-axis will be obtained. The differential transform of Eq. (27) is written in Eq. (45). The first natural frequencies of simply supported higher order shear deformable FGB subjected to axial load can be obtained by solving Eq. (45) in terms of ω.

$$\begin{gathered}m_0\omega^2+b\sum_{k=1}^{m}\Psi(k)k\int_{-c_b}^{c_t}Gy^{k-1}dy\\ +\bar{m}^2\pi^2P/L^2=0\end{gathered} \tag{45}$$

3.3 Collocation method

The collocation method is used as an alternative method to have a faster convergence for large amounts of the material exponent parameter. The differential equation will be converted to a system of algebraic equations. The Taylor series expansion of ψ up to m degree is selected as the finite-dimensional space of candidate solution and the points y_i are selected as the collocation points. Two boundary conditions (44) implies that

$$\begin{gathered}\Psi(1)=h\sum_{k=2}^{[m/2]}\Psi(2k)k\left(\frac{h}{2}\right)^{2k-2}-\sum_{k=3}^{m}\Psi(k)k\left(\frac{h}{2}\right)^{k-1}\\ \Psi(2)=-\sum_{k=2}^{[m/2]}\Psi(2k)k\left(\frac{h}{2}\right)^{2k-2}\end{gathered} \tag{46}$$

where $[m/2]$ denotes floor of $m/2$. Substituting Eq. (39) and Eqs. (46) into Eq. (25) at y_i, yields

$$\begin{gathered}(\rho_i\omega^2L^2-\bar{m}^2\pi^2E_i)\bar{m}^2\pi^2y_i+\xi_0\,\Psi(0)+\\ \xi_1\left(h\sum_{k=2}^{\left[\frac{m}{2}\right]}\Psi(2k)k\left(\frac{h}{2}\right)^{2k-2}-\sum_{k=3}^{m}\Psi(k)k\left(\frac{h}{2}\right)^{k-1}\right)-\xi_2\\ \sum_{k=2}^{\left[\frac{m}{2}\right]}\Psi(2k)k\left(\frac{h}{2}\right)^{2k-2}+\sum_{k=3}^{m}\Psi(k)\big((\rho_i\omega^2L^2-\bar{m}^2\pi^2E_i)\\ L^2y_i^k+G_iL^4k(k-1)y_i^{k-2}+G_{,y}\big|_{y=y_i}L^4ky_i^{k-1}\big)=0\end{gathered} \tag{47}$$

in which the parameters ξ_0 to ξ_2 are presented in Eq. (48).

$$\begin{gathered}\xi_0=(\rho_i\omega^2L^2-\bar{m}^2\pi^2E_i)L^2\\ \xi_1=(\rho_i\omega^2L^4-\bar{m}^2\pi^2L^2E_i)y_i+G_{,y}\big|_{y=y_i}L^4\\ \xi_2=2G_{,y}\big|_{y=y_i}L^4y_i+2G_iL^4+L^2y_i^2\end{gathered} \tag{48}$$

$$(\rho_i \omega^2 L^2 - \bar{m}^2 \pi^2 E_i) \quad (48)$$

The subscript i denotes the value of function at $y = y_i$. The symmetrical collocation points about origin, y_i, are assumed as follows

$$y_i = \left(\frac{i}{m-2} - \frac{m}{2(m-2)}\right) h \quad 1 \le i \le m-1 \quad (49)$$

The unknown parameters $\Psi(0)$ and $\Psi(3)$ to $\Psi(\mathrm{m})$ are obtained by solving system of algebraic equations in Eq. (47) at y_i. The first modes of natural frequencies of simply supported higher order shear deformable FGB subjected to axial load can be obtained by considering Eq. (45).

The similar procedure can be used to solve the stability problem of higher order shear deformable FGB. The symmetrical collocation points about origin, y_i, in Eq. (49) are considered. The unknown parameters $\Phi(0)$ and $\Phi(1)$ in Eq. (32) are obtained by considering Eq. (37).

$$\begin{gathered} \Phi(0) = -\sum_{k=1}^{[m/2]} \Phi(2k) \left(\frac{h}{2}\right)^{2k} \\ \Phi(1) = \frac{2}{h}\left(\sum_{k=1}^{[m/2]} \Phi(2k) \left(\frac{h}{2}\right)^{2k} - \sum_{k=2}^{m} \Phi(k) \left(\frac{h}{2}\right)^{k}\right) \end{gathered} \quad (50)$$

Substituting Eq. (32) and Eqs. (50) into Eq. (16) at y_i, yields

$$\begin{gathered} -\tilde{\xi}_0 \sum_{k=1}^{[m/2]} \Phi(2k) \left(\frac{h}{2}\right)^{2k} + \frac{2\tilde{\xi}_1}{h} \\ \left(\sum_{k=1}^{\left[\frac{m}{2}\right]} \Phi(2k) \left(\frac{h}{2}\right)^{2k} - \sum_{k=2}^{m} \Phi(k) \left(\frac{h}{2}\right)^{k}\right) \\ + \sum_{k=2}^{m} \Phi(k) \left(k(k-1) y^{k-2} + \left.\frac{E_{,y}}{E}\right|_{y=y_i} k y^{k-1} + \tilde{\xi}_0 y^k\right) \\ + 2\beta(1+\nu) = 0 \end{gathered} \quad (51)$$

The parameters $\tilde{\xi}_0$ and $\tilde{\xi}_1$ are defined as follows

$$\begin{gathered} \tilde{\xi}_0 = \left.\left(\frac{E_{,yy}}{E} - \left(\frac{E_{,y}}{E}\right)^2\right)\right|_{y=y_i} - 2\beta(1+\nu) \\ \tilde{\xi}_1 = \left.\frac{E_{,y}}{E}\right|_{y=y_i} + \tilde{\xi}_0 y_i \end{gathered} \quad (52)$$

The unknown parameters $\Phi(2)$ to $\Phi(m)$ are obtained by solving system of algebraic equations in Eq. (51) at y_i. The first modes of buckling loads of higher order shear deformable FGB having various boundary conditions can be obtained by considering Eq. (38).

4. Nonlocal elasticity theory

In the nonlocal elasticity theory the stress tensor at a point depends to strain tensor at all points in domain of the material. The validity of this theory is approved by the experimental observations and atomistic simulation results on phonon dispersion. In the nonlocal elasticity theory the stress-strain relationship has an integral form. Eringen chooses an appropriate kernel function to convert the integral form into the equivalent differential form. In the nonlocal differential elasticity, the differential constitutive equations of higher order shear deformable FGB are as follows (Ebrahimi and Barati 2016)

$$\begin{gathered} \left(1 - \eta^2 \frac{d^2}{(dx)^2}\right) \sigma_{xx}^N = \sigma_{xx} \\ \left(1 - \eta^2 \frac{d^2}{(dx)^2}\right) \tau_{xy}^N = \tau_{xy} \end{gathered} \quad (53)$$

in which σ_{xx}^N and τ_{xy}^N are stress field of nonlocal and σ_{xx} and τ_{xy} are stress field of local FGB respectively. Also, the small scale effects are captured by the scale coefficient, $\eta = \sqrt{\mu}$. Differentiating with respect to x and integrating over the cross section from shear stress in Eq. (53), yields

$$\frac{\partial}{\partial x} \int \tau_{xy}^N \, dA - \eta^2 \frac{\partial^2}{\partial x^2} \left(\frac{\partial}{\partial x} \int \tau_{xy}^N \, dA\right) = \frac{\partial}{\partial x} \int \tau_{xy} \, dA \quad (54)$$

For buckled FGB, by considering Eq. (8), we get

$$P^N w_{,xx} - \eta^2 \frac{\partial^2}{\partial x^2} \left(P^N w_{,xx}\right) = P w_{,xx} \quad (55)$$

By considering the relation $w_{,xxx} = -\beta w_{,x}$ and the Eq. (55), the buckling load of nonlocal FGB, P^N, is obtained in terms of buckling load of local FGB, P.

$$P^N = \frac{P}{1 + \eta^2 \beta} \quad (56)$$

Neglecting axial force and considering Eq. (17), Eqs. (24) and (54), one has

$$\begin{gathered} (\omega^N)^2 \sin\left(\frac{\pi x}{L}\right) - \eta^2 \frac{\partial^2}{\partial x^2} \left((\omega^N)^2 \sin\left(\frac{\pi x}{L}\right)\right) = \\ \omega^2 \sin\left(\frac{\pi x}{L}\right) \end{gathered} \quad (57)$$

The relation between nonlocal circular frequency of vibration, ω^N and local circular frequency of vibration, ω is obtained from Eq. (57) as follows

$$\omega^N = \frac{\omega}{\sqrt{1 + \bar{m}^2 \pi^2 \left(\frac{\eta}{L}\right)^2}} \quad (58)$$

5. Results and discussion

For conducting numerical exercises, the effective material properties of FGB are expressed in Section 5.1. After introducing two homogenization schemes, the comparison and validation by comparing present results with the results of previous works are presented in Section

5.2. The new numerical results for various amounts of slenderness ratio, scale coefficient, material constant, Poisson's ratio and boundary conditions are presented in Section 5.3.

5.1 Effective material properties

It is assumed that the local and nonlocal FGBs are made up of ceramic and metal. The effective bulk modulus and shear modulus based on Mori–Tanaka homogenization technique can be obtained from Eq. (59) (Şimşek and Reddy 2013)

$$\frac{K_e - K_m}{K_c - K_m} = \frac{V_c}{1 + \frac{V_m (K_c - K_m)}{K_m + \frac{4\mu_m}{3}}}$$
$$\frac{\mu_e - \mu_m}{\mu_c - \mu_m} = \frac{V_c}{1 + \frac{V_m (\mu_c - \mu_m)}{\mu_m \left(1 + \frac{9K_m + 8\mu_m}{6K_m + 12\mu_m}\right)}} \tag{59}$$

where the subscripts m and c denote the metallic and ceramic constituents respectively. The effective modulus of elasticity and Poisson's ratio are presented in terms of bulk and shear moduli as follows

$$E(y) = \frac{9K_e\mu_e}{3K_e + \mu_e}$$
$$\nu(y) = \frac{3K_e - 2\mu_e}{6K_e + 2\mu_e} \tag{60}$$

The effective modulus of elasticity and mass density based on classical rule of mixture are

$$E(y) = E_m V_m + E_c V_c$$
$$\rho(y) = \rho_m V_m + \rho_c V_c \tag{61}$$

The volume fraction of the phase materials are presented in Eq. (62).

$$V_c = \left(\frac{1}{2} + \frac{y}{h}\right)^n$$
$$V_m = 1 - \left(\frac{1}{2} + \frac{y}{h}\right)^n \tag{62}$$

Table 2 The convergence of results for FGB (n = 1)

m	Critical load ($\bar{P}_1, L/h = 20$)		Fundamental frequency ($\bar{\omega}_1, L/h = 5$)	
	DTM	CM	DTM	CM
0	41.8524442	42.2787109	3.9838762	3.9912844
15	41.8322576	41.9545456	3.9897744	3.9900182
20	41.9356992	41.9498883	3.9898571	3.9900099
25	41.9322170	41.9477374	3.9900027	3.9900083
30	41.9460639	41.9476919	3.9900046	3.9900083
40	41.9474434	41.9476580	3.9900083	-
50	41.9476286	41.9476574	-	-
80	41.9476574	41.9476574	-	-

where n is material exponent parameter or gradient index which takes non-negative real numbers. Also, h is the height of rectangular section. In above-mentioned two homogenization methods the bottom and top surfaces of FGB are pure metal and pure ceramic respectively.

5.2 Comparison and validation

The convergence of differential transform method (DTM) and collocation method (CM) for numerical solutions of free vibration and stability problems of higher order shear deformable FGB is presented in Table 2. The dimensionless parameters $\bar{P}_1$ and $\bar{\omega}_1$ are equal to $PL^2/E_m I$ and $\omega L^2\sqrt{\rho_m/E_m h^2}$ respectively. The parameter I is cross section's moment of inertia. For calculating the numerical amounts of $\bar{P}_1$, the ratio of E_c to E_m and Poison's ratio are assumed equal to 10 and 0.38 respectively. For calculating the numerical amounts of $\bar{\omega}_1$, it is assumed that the FGB composed of alumina ($E_c =$ 380 GPa, $\rho_c = 3960$ kg/m^3) and aluminium ($E_m =$ 70 GPa, $\rho_m = 2702$ kg/m^3) with the constant Poisson's ratio equal to 0.3. The fundamental circular frequencies of free vibration are calculated by neglecting the axial force. The rate of convergence for numerical results based on CM is more than the rate of convergence based on DTM. Moreover, the rate of convergence for vibration analysis is more than buckling analysis. Table 3 shows the validity of numerical results for simply supported higher order homogeneous nanobeam by considering various amounts of slenderness ratios and scale coefficients. The length of the nanobeam and Poisson's ratio are assumed equal to 10 nm and 0.3 respectively. The dimensionless parameter $\bar{\omega}_2$ is equal to $\omega L^2\sqrt{\rho A/EI}$, in which EI is flexural rigidity of the beam. The result validation of homogeneous nonlocal beam having pinned ends for second and third free vibration modes are presented in Table 4.

By decreasing slenderness ratio and scale coefficient and increasing mode's number the difference between results of current work and the outcomes of Thai and Vo (2012b) is increased. The results in Tables 3 and 4 show that the present method gives less frequencies and less buckling loads than the results of Thai and Vo (2012b) due to considering the exact through-thickness distribution of shear strain and exact position of neutral-axis in higher order shear deformable beam. The result validation for buckling analysis of higher order shear deformable homogeneous nanobeam having pinned (S-S) and clamped (C-C) end conditions is presented by comparing our results with the results of third order Reddy homogeneous nanobeams in Table 5. The results based on current work show a good agreement with the results of Reddy theory (Emam 2013). The result validation for buckling analysis of shear deformable simply supported FGB is presented in Table 6. For conducting numerical exercises the mechanical properties of FGB are assumed similar to the mechanical properties that are introduced for calculating $\bar{P}_1$ in Table 2. The non-dimensional critical loads of current work for pinned inhomogeneous and homogeneous local beams are less than the results of Reddy (2011) and Şimşek and Reddy(2013). The critical loads of shear deformable pinned

Table 3 Result validation for higher order shear deformable homogeneous nanobeam

L/h	$\mu(nm^2)$	Critical load ($\bar{P}_1$)		Fundamental frequency ($\bar{\omega}_2$)	
		Thai and Vo (2012b)	Current work	Thai and Vo (2012b)	Current work
5	0	8.9533	8.9518	9.2752	9.2745
	1	8.1490	8.1477	8.8488	8.8481
	2	7.4773	7.4761	8.4763	8.4756
	3	6.9079	6.9068	.1472	8.1465
	4	6.4191	6.4180	7.8536	7.8530
10	0	9.6231	9.6227	9.7077	9.7075
	1	8.7587	8.7583	9.2614	9.2612
	2	8.0367	8.0364	8.8715	8.8713
	3	7.4247	7.42445	8.5271	8.5268
	4	6.8994	6.8990	8.2198	8.2196
20	0	9.8068	9.8066	9.8282	9.8281
	1	8.9258	8.9257	9.3764	9.3763
	2	8.1901	8.1900	8.9816	8.9815
	3	7.5665	7.5663	8.6329	8.6328
	4	7.0310	7.0309	8.3218	8.3218
100	0	9.8671	9.8671	9.8679	9.8679
	1	8.9807	8.9807	9.4143	9.4142
	2	8.2405	8.2404	9.0180	9.0179
	3	7.6130	7.6129	8.6678	8.6678
	4	7.0743	7.0742	8.3555	8.3555

Table 4 Result validation for higher modes of higher order shear deformable homogeneous nanobeam

L/h	$\mu(nm^2)$	Critical load ($\bar{P}_1$)		Fundamental frequency ($\bar{\omega}_2$)	
		Thai and Vo (2012b)	Current work	Thai and Vo (2012b)	Current work
5	0	32.1948	32.1840	61.6192	61.5662
	1	27.2604	27.2513	44.8420	44.8034
	2	24.0664	24.0584	36.9798	36.9480
	3	21.7833	21.7760	32.1878	32.1 01
	4	20.0470	2 .0402	28.8778	28.8530
10	0	37.1009	37.0980	78.1855	78.1715
	1	31.4146	31.4121	56.8977	56.8875
	2	27.7339	27.7317	46.9219	46.9135
	3	25.1029	25.1009	40.8415	40.8342
	4	23.1019	23.1001	36.6416	36.6350
20	0	38.8308	38.8300	85.6671	85.6634
	1	32.8793	32.8786	62.3422	62.3395
	2	29.0270	29.0264	51.4118	51.4096
	3	26.2733	26.2728	44.7496	44.7477
	4	24.1790	24.1785	40.1478	40.1461
100	0	39.4517	39.4516	88.6915	88.6913
	1	33.4051	33.4050	64.5432	64.5430
	2	29.4912	29.4911	53.2269	53.2267
	3	26.6934	26.6934	46.3295	46.3293
	4	24.5657	24.5656	41.5653	41.5651

Table 5 Result validation for higher order homogeneous nanobeam having various end conditions

L/h	μ	Critical load ($\bar{P}_1$,S-S)		Critical load ($\bar{P}_1$,C-C)	
		Emam (2013)	Current work	Emam (2013)	Current work
10	0	9.6228	9.6227	35.8075	35.8074
	1	8.7583	8.7583	25.6724	25.6723
	2	8.0364	8.0364	20.0090	20.0089
	3	7.4245	7.4244	16.3927	16.3927
	4	6.8991	6.8990	13.8835	13.8834
	5	6.4432	6.4431	12.0405	12.0404
20	0	9.8067	9.8066	38.4910	38.4910
	1	8.9258	8.9257	27.5964	27.5963
	2	8.1900	8.1900	21.5085	21.5085
	3	7.5664	7.5663	17.6212	17.6212
	4	7.0310	7.0309	14.9240	14.9239
	5	6.5663	6.5663	12.9429	12.9428

Table 6 Result validation for critical load of higher order shear deformable FGB (L/h = 20)

$n=0$			$n=1$			$n=10$		
Reddy (2011)	Şimşek and Reddy (2013)	Current work ($\bar{P}_1$)	Reddy (2011)	Şimşek and Reddy(2013)	Current work ($\bar{P}_1$)	Reddy (2011)	Şimşek and Reddy(2013)	Current work ($\bar{P}_1$)
9.81	9.8058	9.8028	41.96	41.9583	41.9476	19.55	19.5523	19.4850

FGBs based on Mori–Tanaka homogenization scheme and many beam models like the first shear deformation theory, trigonometric shear deformation theory and exponential shear deformation theory are calculated by the Şimşek and Reddy (2013). The results based on hyperbolic shear deformation theory and parabolic shear deformation theory are less than or equal to the results based on the proposed theory of Şimşek and Reddy and other mentioned theories. The difference between Poisson's ratio of ceramic and metallic constituents are negligible($\nu_m = 0.3177,\ \nu_c = 0.3$), therefore the results based on current work are presented for constant Poisson's ratio and variable modulus of elasticity which is obtained by using Mori–Tanaka scheme ($E_m = 210$ GPa, $E_c = 390$ GPa). By approaching material exponent parameter to 10, the through-thickness distribution of Poisson's ratio is approached to ν_m. Table 7

Table 7 Critical load of higher order shear deformable FGB based on various effective material properties (L/h = 20)

n	Method	ν	$\bar{P}_1$ based on MT	$\bar{P}_1$ based on CR
1	Current work	ν_m	13.2909	13.5906
		ν_c	13.2920	13.5917
		$\nu_{ave.}$	13.2914	13.5912
	PSDT (Şimşek and Reddy 2013)	$\nu_{var.}$	13.2916	-
2	Current work	ν_m	12.4922	12.6981
		ν_c	12.4933	12.6993
		$\nu_{ave.}$	12.4927	12.6987
	PSDT (Şimşek and Reddy 2013)	$\nu_{var.}$	12.4927	-
5	Current work	ν_m	11.7250	11.9302
		ν_c	*11.7262*	*11.9314*
		$\nu_{ave.}$	*11.7256*	*11.9308*
	PSDT (Şimşek and Reddy 2013)	$\nu_{var.}$	11.7252	-
10	Current work	ν_m	11.1402	11.3283
	PSDT (Şimşek and Reddy 2013)	$\nu_{var.}$	*11.1403*	-

Table 8 Through the thickness variation of shear strains in higher order beam theories

Beam model	Shape function of shear strain (g)
TBT	$1-\left(\frac{y}{h/2}\right)^2$
SBT	$cos\left(\frac{\pi y}{h}\right)$
HBT	$cosh\left(\frac{y}{h}\right)-cosh\left(\frac{1}{2}\right)$
EBT	$\left(1-\left(\frac{y}{h/2}\right)^2\right)e^{-2\left(\frac{y}{h}\right)^2}$
CBT	0

shows a good agreement between the critical loads of higher order shear deformable FGBs based on current work and based on parabolic shear deformation theory (PSDT). The results show that new proposed method can be used for exact analysis of arbitrary material gradations like the classical rule of mixture (CR) and Mori–Tanaka (MT) homogenizations schemes. The critical load is decreased by increasing Poisson's ratio. Moreover it can be seen that when the average of Poisson's ratios of metal and ceramic is used, the critical load is approached to the average of critical loads of metallic and ceramic beams. The shear strain for various beam theories is assumed as $gw_{s,x}$, where g and w_s are the shape function and shear component of transverse displacement respectively. The shape function of shear strain for third-order beam theory (TBT), sinusoidal beam theory (SBT), hyperbolic beam theory (HBT), exponential beam theory (EBT) and Euler-Bernoulli or classical beam theory (CBT) are shown in Table 8 (Thai and Vo 2012a).

Shear stress-free conditions at top and bottom fibres of FGB in all mentioned models are satisfied. By increasing slenderness ratio the effect of shear strain on vibration behavior of FGB is decreased. Therefore a good agreement between the results of various theories is observed for the large amounts of slenderness ratio. Based on various beam theories the fundamental natural circular frequencies of higher order simply supported local FGBs for various slenderness ratio and material exponent parameter are calculated by Thai and Vo (2012a). The outcomes of present paper are compared by the results of various beam models in Table 9. For conducting numerical exercises the mechanical properties of FGB are assumed equal to the mechanical properties which are introduced for calculating $\bar{\omega}_1$ in Table 2.

The frequencies of local FGBs ($n \neq 0$) based on current work are less than the frequencies based on TBT, SBT, HBT, EBT and CBT. Therefore our proposed method improves the results of previous works. The validity of vibration analysis for higher order shear deformable FG nanobeam is presented in Table 10 by considering various amounts of slenderness ratio, scale coefficient and material exponent parameter. The results are compared with the both, nonlocal Timoshenko beam theory (Rahmani and Pedram 2014) and nonlocal higher order beam theory (Ebrahimi and Barati 2016). The dimensionless parameter $\bar{\omega}_2$ is equal to $\omega L^2\sqrt{\rho_c A/E_c I}$, in which I is cross section's moment of inertia. For numerical examples the mechanical properties of FGB are assumed as ($E_c =$ 390 GPa, $\rho_c = 3960\ \mathrm{kg/m^3}$) for ceramic and ($E_m =$ 210 GPa, $\rho_m = 7800\ \mathrm{kg/m^3}$) for metallic materials. In addition, the Poisson's ratio is taken to be constant ($\nu =$ 0.3). The calculated frequencies based on current work are less than calculated frequencies based on mentioned works in Table 10. Therefore the proposed method in current work improves the results of previous works.

5.2 Numerical results

In all cases, when no assumptions are mentioned, the slenderness ratio, length of nanobeam, scale coefficient, gradient index and Poisson's ratio are assumed equal to 20, 10 nm, 2, 1 and 0.3 respectively. Also, the mechanical properties of FGB are ($E_c = 390$ GPa, $\rho_c = 3960\ \mathrm{kg/m^3}$) for ceramic and ($E_m = 210$ GPa, $\rho_m = 7800\ \mathrm{kg/m^3}$) for metallic materials. Also, when end conditions aren't

Table 9 Result validation for vibration analysis of higher order shear deformable FGB

L/h	n	TBT	SBT	HBT	EBT	CBT	Current work ($\bar{\omega}_1$)
5	0.0	5.1527	5.1531	5.1527	5.1542	5.3953	5.1527
	0.5	4.4107	4.4110	4.4107	4.4118	4.5931	4.4098
	1.0	3.9904	3.9907	3.9904	3.9914	4.1484	3.9900
	2.0	3.6264	3.6263	3.6265	3.6267	3.7793	3.6237
	5.0	3.4012	3.3998	3.4014	3.3991	3.5949	3.3975
	10.0	3.2816	3.2811	3.2817	3.2814	3.4921	3.2800
20	0.0	5.4603	5.4603	5.4603	5.4604	5.4777	5.4603
	0.5	4.6511	4.6511	4.6511	4.6512	4.6641	4.6500
	1.0	4.2051	4.2051	4.2051	4.2051	4.2163	4.2050
	2.0	3.8361	3.8361	3.8361	3.8361	3.8472	3.8359
	5.0	3.6485	3.6484	3.6485	3.6483	3.6628	3.6481
	10.0	3.5390	3.5389	3.5390	3.5390	3.5547	3.5387

Table 10 Comparison of current work results with the results of Timoshenko and higher order FG nano-beams

L/h		μ	$n=0$	$n=0.2$	$n=0.5$	$n=1$	$n=2$	$n=5$	$n=10$
20	Ebrahimi and Barati (2016)	0	9.829569	8.660194	7.715125	6.967613	6.395955	5.916152	5.651341
		1	9.377686	8.262069	7.360447	6.64730	6.101922	5.644175	5.391538
		2	8.982894	7.914243	7.050579	6.367454	5.845036	5.406561	5.164560
		3	8.634103	7.606946	6.776816	6.120217	5.618083	5.196632	4.964028
		4	8.323021	7.332872	6.532651	5.899708	5.415670	5.009400	4.785177
	Rahmani and Pedram (2014)	0	9.8296	8.6600	7.7149	6.9676	-	5.9172	5.6521
		1	9.3777	8.2620	7.3602	6.6473	-	5.6452	5.3923
		2	8.9829	7.9140	7.0504	6.3674	-	5.4075	5.1653
		3	8.6341	7.6068	6.7766	6.1202	-	5.1975	4.9647
		4	8.3230	7.3327	6.5325	5.8997	-	5.0103	4.7858
	Current work ($\bar{\omega}_2$)	0	9.828129	8.6579	7.7126	6.966932	6.395479	5.915990	5.651284
		1	9.376312	8.2598	7.3580	6.646650	6.101467	5.644021	5.391484
		2	8.981578	7.9121	7.0483	6.366832	5.844601	5.406413	5.164507
		3	8.632838	7.6049	6.7745	6.119618	5.617664	5.196490	4.963978
		4	8.321801	7.3309	6.5305	5.899131	5.415263	5.009264	4.785128
50	Ebrahimi and Barati (2016)	0	9.863157	8.68958	7.74135	6.99174	6.41911	5.93877	5.67285
		1	9.409730	8.29010	7.38547	6.67032	6.12401	5.66576	5.41206
		2	9.013589	7.94110	7.07455	6.38950	5.86620	5.42723	5.18421
		3	8.663606	7.63276	6.79985	6.14141	5.63842	5.21650	4.98292
		4	8.351461	7.35775	6.55486	5.92014	5.43527	5.02855	4.80340
	Rahmani and Pedram (2014)	0	9.8631	8.6895	7.7413	6.9917	-	5.9389	5.6730
		1	9.4097	8.2901	7.3854	6.6703	-	5.6659	5.4122
		2	9.0136	7.9411	7.0745	6.3895	-	5.4274	5.1843
		3	8.6636	7.6327	6.7998	6.1414	-	5.2166	4.9830
		4	8.3515	7.3577	6.5548	5.9201	-	5.0287	4.8035
	Current work ($\bar{\omega}_2$)	0	9.862924	8.6882	7.7396	6.991629	6.419034	5.938746	5.672837
		1	9.409508	8.2887	7.3837	6.670211	6.123939	5.665731	5.412046
		2	9.013376	7.9398	7.0729	6.389401	5.866127	5.427209	5.184204
		3	8.663400	7.6315	6.7983	6.141311	5.638354	5.216479	4.982909
		4	8.351263	7.3565	6.5533	5.920043	5.435207	5.028532	4.803378
100	Ebrahimi and Barati (2016)	0	9.86799	8.69381	7.74513	6.99521	6.42245	5.94203	5.67594
		1	9.41434	8.29414	7.38907	6.67363	6.12719	5.66886	5.41501
		2	9.01801	7.94496	7.0780	6.39268	5.86925	5.43021	5.18704
		3	8.66785	7.63647	6.80317	6.14446	5.64135	5.21936	4.98564
		4	8.35555	7.36133	6.55805	5.92308	5.43810	5.03131	4.80601
	Rahmani and Pedram (2014)	0	9.8680	8.6938	7.7451	6.9952	-	5.9421	5.6760
		1	9.4143	8.2941	7.3891	6.6736	-	5.6689	5.4150
		2	9.0180	7.9449	7.0780	6.3927	-	5.4302	5.1871
		3	8.6678	7.6365	6.8032	6.1444	-	5.2194	4.9857
		4	8.3555	7.3613	6.5580	5.9231	-	5.0313	4.8060
	Current work ($\bar{\omega}_2$)	0	9.867932	8.6926	7.7440	6.995184	6.422426	5.942023	5.675941
		1	9.414285	8.2929	7.3879	6.673603	6.127175	5.668857	5.415008
		2	9.017952	7.9438	7.0769	6.392650	5.869227	5.430204	5.187041
		3	8.667799	7.6354	6.8021	6.144433	5.641334	5.219357	4.985636
		4	8.355503	7.3603	6.5571	5.923053	5.438080	5.031307	4.806006

mentioned, it is assumed that the boundary condition is simply supported. The flexural rigidity of Euler-Bernoulli FGB, EI_{FG}, and mass of unit length, m_0, are used to normalize the buckling loads and natural frequencies. The flexural rigidity of thin FGB according to the power-law distribution of the volume fraction of the constituents can be obtained easily as follows (Heydari 2011)

$$EI_{FG} = (E_m^2 n^4 + 4E_m(E_c + E_m)n^3 + (16E_cE_m + 7E_m^2)n^2 + 28E_cE_m n + 12E_c^2)I/\left((n+3)(n+2)^2(nE_m + E_c)\right) \tag{63}$$

where the parameter I is cross section's moment of inertia. The dimensionless parameters $\bar{P}_2$ and $\bar{\omega}_3$ are equal to $PL^2/(\pi^2 EI_{FG})$ and $\omega L^2\sqrt{m_0/(\pi^4 EI_{FG})}$ respectively, which for simply supported thin FGB are equal to one. The effect of Poisson's ratio on critical load of higher order shear deformable local FGB for various amounts of length to thickness ratios is illustrated in Fig. 2. The critical load is decreased by increasing Poisson's ratio. The effect of Poisson's ratio on buckling load of thin FGB is negligible. By decreasing slenderness ratio the dimensionless buckling load is decreased due to shear deformation effect. The effect of Poisson's ratio on critical load of higher order shear deformable nonlocal FGB for various amounts of scale coefficient is presented in Fig. 3. The slenderness ratio is assumed equal to 5. By increasing scale coefficient and Poisson's ratio the critical load is decreased.

Fig. 4 illustrates the effect of E_c to E_m ratio on non-dimensional buckling load of higher order shear deformable nonlocal FGB for various amounts of material exponent parameter. The dimensionless critical load is decreased by increasing gradient index.

The first four non-dimensional buckling loads of higher order FG nanobeam for simply clamped (S-C) end condition and various amounts of E_c to E_m ratio are illustrated in Fig. 5. For higher modes the effect of small scale on buckling load is increased.

The effect of axial load on first three natural frequencies of higher order shear deformable FGB is illustrated in Fig. 6. The sign of axial compression is taken to be positive. The slenderness ratio is assumed equal to 5. The compressive axial load decreases the natural frequency and tensile axial load increases the natural frequency of higher order shear deformable FG nanobeam. By approaching the axial compression to the buckling load, the natural frequency of corresponding mode approaches to zero.

The fundamental frequency of higher order shear deformable FGB based on two homogenization schemes, the Mori–Tanaka technique (MT) and classical rule of mixture (CR) for various amounts of slenderness ratio is

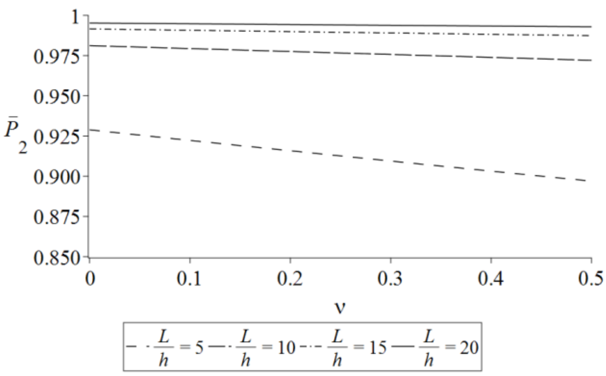

Fig. 2 The effects of Poisson's ratio and slenderness ratio on critical load of higher order FGB

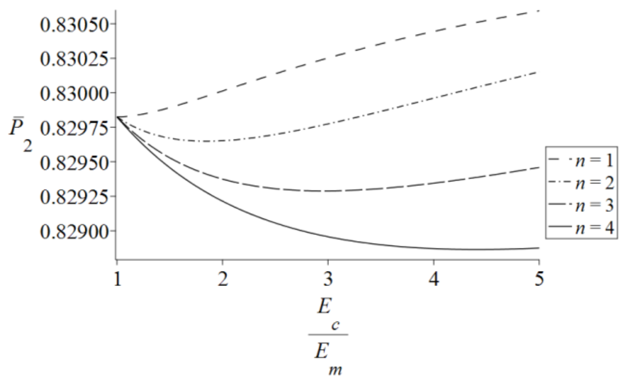

Fig. 4 The effects of E_c to E_m ratio and gradient index on critical load of higher order shear deformable nonlocal FGB

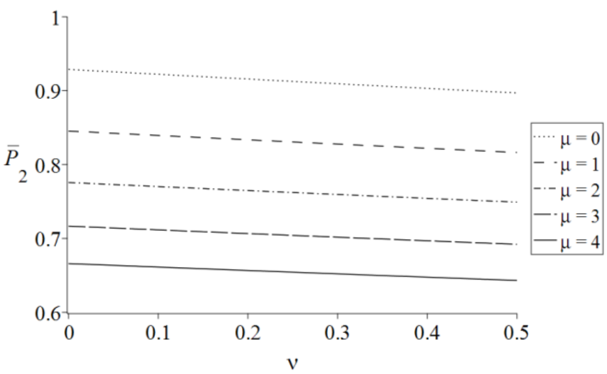

Fig. 3 The effects of Poisson's ratio and scale coefficient on critical load of higher order shear deformable nonlocal FGB ($L = 5h$)

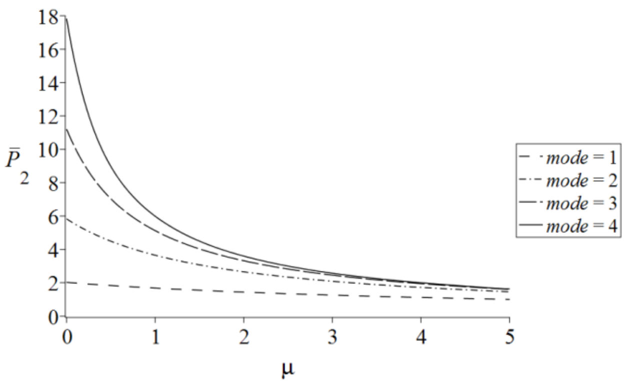

Fig. 5 The first four dimensionless buckling loads of simply clamped (S-C) higher order shear deformable nonlocal FGB

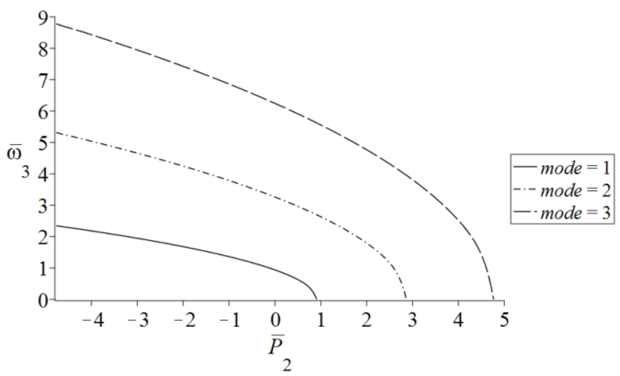

Fig. 6 The effect of axial load on first three dimensionless frequencies of higher order FGB ($L = 5h$)

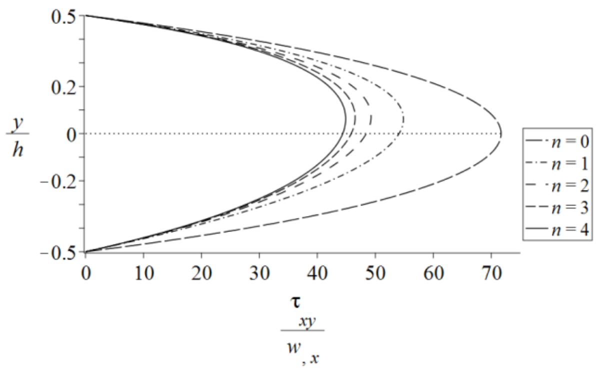

Fig. 9 Profile of shear stress for various amounts of gradient index ($L = 2h$)

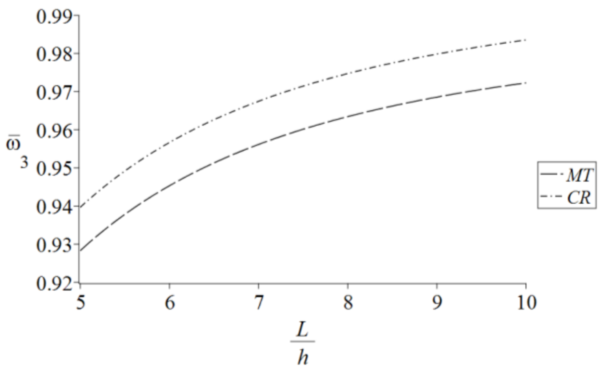

Fig. 7 The fundamental natural frequency based on MT and CR homogenization schemes

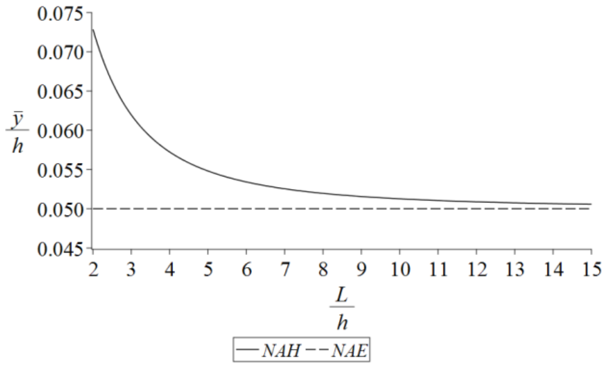

Fig. 10 The difference between positions of neutral axis for thin and thick FGBs

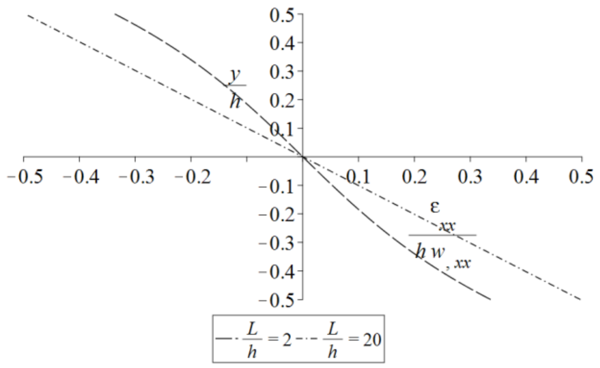

Fig. 8 Profile of axial strain for various amounts of slenderness ratio ($n = 0$)

plotted in Fig. 7. The Poisson's ratio is taken to be constant. For both cases, the Eq. (63) is used to normalize the fundamental frequency. The MT scheme gives the less frequencies than CR method.

The axial strain of buckled higher order shear deformable homogeneous beam ($n = 0$) for various slenderness ratios are presented in Fig. 8. By increasing slenderness ratio, the nonlinear distribution of axial strain is transformed to a linear distribution. In addition, the shear stress of higher order buckled FGB for various material exponent parameters are illustrated in Fig. 9. In contrast to the FGB, the maximum shear stress of higher order shear deformable homogeneous beam is occurred at mid-axis.

The axial displacement (axial strain or axial stress) of higher order shear deformable FGB for first mode of vibration is set equal to zero to find the position of neutral axis. The position of neutral axis ($\bar{y}$) is measured from the mid-axis. Fig. 10 presents the location of neutral axis for higher order shear deformable FGB (NAH) and location of neutral axis for Euler-Bernoulli FGB (NAE). By increasing the slenderness ratio NAH approaches to the NAE, which indicates that the results of current work are valid. It is noteworthy to mention that the exact shear stress takes the maximum value at neutral axis (NAH), whereas in earlier higher order shear deformation beam theories the maximum shear strain usually is occurred at mid-axis (Table 8). Moreover, the neutral axis for shear deformable FGB is located somewhere rather than the position of neutral axis for Euler-Bernoulli FGB. Therefore the methodology of current work not only improves the previous works based on the various higher order shear deformation beam theories but also improves the vibration and buckling analyses for shear deformable FGB by considering exact position of neutral axis instead of using position of neutral axis for Euler-Bernoulli FGB (Eltaher *et al.* 2014).

6. Conclusions

Survey in the literature, shows that the previous works about the vibration and buckling analyses of shear deformable homogeneous and heterogeneous beams have two main weaknesses. Firstly, they guess some shear strain shape functions instead of using exact through-thickness distribution of shear strain, secondly, some works used the position of neutral axis of Euler-Bernoulli FGB instead of exact position of neutral axis. The present paper intended to find an exact shear strain shape function and avoided to guess a shape function for across-the-thickness variation of shear strain. As a result, for the first time, the exact position of neutral axis for vibration and buckling analyses of higher order shear deformable FG and homogeneous nanobeams is considered. The exact shear stress takes the maximum value at neutral axis, whereas in earlier higher order shear deformation beam theories the maximum shear strain usually is occurred at mid-axis. The methodology of current work not only improved the previous works based on the various higher order shear deformation beam theories but also the vibration and buckling analyses for shear deformable FGB by considering exact position of neutral axis instead of using position of neutral axis for Euler-Bernoulli FGB developed. The new approaches based on separation of shear strain into two independent variables is proposed to solve the coupled partial differential equations of motion for arbitrary material gradation without any simplification. In numerical analyses, the faster convergence is observed by using differential transformation and collocation methods for fractional values and great amounts of gradient index, respectively. For the homogeneous beams, the exact new formulas are obtained. The analytical relations between nonlocal and local buckling loads and natural frequencies are obtained using Eringen's nonlocal continuum theory. The exact buckling loads of first modes for various classical end conditions and natural frequencies of first modes for pinned ends are calculated. For similar gradient index, the Mori-Tanaka homogenization scheme gives smaller buckling loads and natural frequencies than the classical rule of mixture. The effect of small scale on buckling load and natural frequency in higher modes is more significant. By approaching the axial compression to the buckling load, the natural frequency of corresponding mode approaches to zero. The normalized buckling loads and natural frequencies decreased by increasing the scale coefficient, thickness to length ratio, material exponent parameter and Poisson's ratio.

References

Abazari, R. (2009), "Solution of Riccati types matrix differential equations using matrix differential transform method", *J. Appl. Math. Inform.*, **27**, 1133-1143.

Amirpour, M., Das, R. and Saavedra Flores, E.I. (2016), "Analytical solutions for elastic deformation of functionally graded thick plates with in-plane stiffness variation using higher order shear deformation theory", *Compos. Part B: Eng.*, **94**, 109-121.

Arikoglu, A. and Ozkol, I. (2005), "Solution of boundary value problems for integro-differential equations by using differential transform method", *Appl. Math. Comput.*, **168**(2), 1145-1158.

Arikoglu, A. and Ozkol, I. (2006), "Solution of differential–difference equations by using differential transform method", *Appl. Math. Comput.*, **181**(1), 153-162.

Arikoglu, A. and Ozkol, I. (2007), "Solution of fractional differential equations by using differential transform method", *Chaos Solit. Fract.*, **34**(5), 1473-1481.

Bayat, M., Pakar, I. and Bayat, M. (2017), "Nonlinear vibration of multi-body systems with linear and nonlinear springs", *Steel Compos. Struct., Int. J.*, **25**(4), 497-503.

Belabed, Z., Houari, M.S.A., Tounsi, A., Mahmoud, S.R. and Bég, O.A. (2014), "An efficient and simple higher order shear and normal deformation theory for functionally graded material (FGM) plates", *Compos. Part B: Eng.*, **60**, 274-283.

Bellifa, H., Bakora, A., Tounsi, A., Bousahla, A.A. and Mahmoud, S.R. (2017), "An efficient and simple four variable refined plate theory for buckling analysis of functionally graded plates", *Steel Compos. Struct., Int. J.*, **25**(3), 257-270.

Bhrawy, A.H., Doha, E.H., Abdelkawy, M.A. and Hafez, R.M. (2015), "An efficient collocation algorithm for multi-dimensional wave type equations with nonlocal conservation conditions", *Appl. Math. Model.*, **39**(18), 5616-5635.

Challamel, N. (2013), "Variational formulation of gradient or/and nonlocal higher-order shear elasticity beams", *Compos. Struct.*, **105**, 351-368.

de Sciarra, F.M. (2013), "A nonlocal finite element approach to nanobeams", *Adv. Mech. Eng.*, **5**, 720406.

Demir, Ç. and Civalek, Ö. (2017), "A new nonlocal FEM via Hermitian cubic shape functions for thermal vibration of nano beams surrounded by an elastic matrix", *Compos. Struct.*, **168**, 872-884.

Ebrahimi, F. and Barati, M.R. (2016), "A nonlocal higher-order shear deformation beam theory for vibration analysis of size-dependent functionally graded nanobeams", *Arab. J. Sci. Eng.*, **41**(5), 1679-1690.

Eltaher, M.A., Abdelrahman, A.A., Al-Nabawy, A., Khater, M. and Mansour, A. (2014), "Vibration of nonlinear graduation of nano-Timoshenko beam considering the neutral axis position", *Appl. Math. Comput.*, **235**, 512-529.

Emam, S.A. (2013), "A general nonlocal nonlinear model for buckling of nanobeams", *Appl. Math. Comput.*, **37**(10-11), 6929-6939.

Eringen, A.C. (1972a), "Nonlocal polar elastic continua", *Int. J. Eng. Sci.*, **10**, 1-16.

Eringen, A.C. (1972b), "Linear theory of nonlocal elasticity and dispersion of plane waves", *Int. J. Eng. Sci.*, **10**, 425-435.

Eringen, A.C. (1978), "Line crack subjected to shear", *Int. J. Fracture*, **14**, 367-379.

Eringen, A.C. (1983), "On differential equations of nonlocal elasticity and solutions of screw dislocation and surface waves", *J. Appl. Phys.*, **54**(9), 4703-4710.

Eringen, A.C. and Edelen, D.G.B. (1972), "On nonlocal elasticity", *Int. J. Eng. Sci.*, **10**(3), 233-248.

Eringen, A.C. and Kim, B.S. (1974), "Stress concentration at the tip of a crack", *Mech. Res. Commun.*, **1**, 233-237.

Eringen, A.C., Speziale, C.G. and Kim, B.S. (1977), "Crack-tip problem in non-local elasticity", *J. Mech. Phys. Solids*, **25**, 339-355.

Ghadiri, M., Shafiei, N. and Babaei, R. (2017), "Vibration of a rotary FG plate with consideration of thermal and Coriolis effects", *Steel Compos. Struct., Int. J.*, **25**(2), 197-207.

Hadji, L., Khelifa, Z. and El Abbes, A.B. (2016), "A new higher order shear deformation model for functionally graded beams", *KSCE J. Civil Eng.*, **20**(5), 1835-1841.

He, G., Wang, D. and Yang, X. (2016), "Analytical solutions for free vibration and buckling of composite beams using a higher order beam theory", *Acta Mechanica Solida Sinica*, **29**(3), 300-315.

Heydari, A. (2011), "Buckling of functionally graded beams with rectangular and annular sections subjected to axial compression", *Int. J. Adv. Des. Manuf. Technol.*, **5**(1), 25-31.

Heydari, A. (2013), "Analytical solutions for buckling of functionally graded circular plates under uniform radial compression by using Bessel function", *Int. J. Adv. Des. Manuf. Technol.*, **6**(4).

Heydari, A. (2015), "Spreading of Plastic Zones in Functionally Graded Spherical Tanks Subjected to Internal Pressure and Temperature Gradient Combinations", *Iran. J. Mech. Eng. Transact. ISME*, **16**(2), 5-25.

Heydari, A. and Shariati, M. (2018), "Buckling analysis of tapered BDFGM nano-beam under variable axial compression resting on elastic medium", *Struct. Eng. Mech., Int. J.*, **66**(6), 737-748.

Heydari, A., Jalali, A. and Nemati, A. (2017), "Buckling analysis of circular functionally graded plate under uniform radial compression including shear deformation with linear and quadratic thickness variation on the Pasternak elastic foundation", *Appl. Math. Model.*, **41**, 494-507.

Hosseini-Hashemi, S., Nazemnezhad, R. and Bedroud, M. (2014), "Surface effects on nonlinear free vibration of functionally graded nanobeams using nonlocal elasticity", *Appl. Math. Model.*, **38**(14), 3538-3553.

Jandaghian, A.A. and Rahmani, O. (2017), "Vibration analysis of FG nanobeams based on third-order shear deformation theory under various boundary conditions", *Steel Compos. Struct., Int. J.*, **25**(1), 67-78.

Karama, M., Afaq, K.S. and Mistou, S. (2003), "Mechanical behaviour of laminated composite beam by the new multi-layered laminated composite structures model with transverse shear stress continuity", *Int. J. Solids Struct.*, **40**(6), 1525-1546.

Karličić, D., Kozić, P. and Pavlović, R. (2015), "Flexural vibration and buckling analysis of single-walled carbon nanotubes using different gradient elasticity theories based on Reddy and Huu-Tai formulations", *J. Theor. Appl. Mech.*, **53**.

Karličić, D., Kozić, P. and Pavlović, R. (2016), "Nonlocal vibration and stability of a multiple-nanobeam system coupled by the Winkler elastic medium", *Appl. Math. Model.*, **40**(2), 1599-1614.

Keskin, Y., Kurnaz, A., Kiris, M.E. and Oturanc, G. (2007), "Approximate solutions of generalized pantograph equations by the differential transform method", *Int. J. Nonlinear Sci. Numer. Simul.*, **8**(2), 159-164.

Koutsoumaris, C.C., Eptaimeros, K.G. and Tsamasphyros, G.J. (2017), "A different approach to Eringen's nonlocal integral stress model with applications for beams", *Int. J. Solids Struct.*, **112**, 222-238.

Li, Y.S., Ma, P. and Wang, W. (2015), "Bending, buckling, and free vibration of magnetoelectroelastic nanobeam based on nonlocal theory", *J. Intel. Mater. Syst. Struct.*, **27**(9), 1139-1149.

Mantari, J.L. and Guedes Soares, C. (2014), "Optimized sinusoidal higher order shear deformation theory for the analysis of functionally graded plates and shells", *Compos. Part B: Eng.*, **56**, 126-136.

Mechab, I. (2009), "Etude des structures composites en utilisant les theories d'ordre élevé sous chargement thermomécanique", University of Sidi Bel Abbes.

Menasria, A., Bouhadra, A., Tounsi, A., Bousahla, A.A. and Mahmoud, S.R. (2017), "A new and simple HSDT for thermal stability analysis of FG sandwich plates", *Steel Compos. Struct, Int. J.*, **25**(2), 157-175.

Mohamed, S.A., Shanab, R.A. and Seddek, L.F. (2016), "Vibration analysis of Euler–Bernoulli nanobeams embedded in an elastic medium by a sixth-order compact finite difference method", *Appl. Math. Model.*, **40**(3), 2396-2406.

Mori, T. and Tanaka, K. (1973), "Average stress in matrix and average elastic energy of materials with mis-fitting Inclusions", *Acta Metal*, **21**, 571-583.

Oskouie, M.F. and Ansari, R. (2017), "Linear and nonlinear vibrations of fractional viscoelastic Timoshenko nanobeams considering surface energy effects", *Appl. Math. Model.*, **43**, 337-350.

Rahmani, O. and Pedram, O. (2014), "Analysis and modeling the size effect on vibration of functionally graded nanobeams based on nonlocal Timoshenko beam theory", *Int. J. Eng. Sci.*, **77**, 55-70.

Reddy, J.N. (1984), "A simple higher-order theory for laminated composite plates", *J. Appl. Mech.*, **51**(4), 745-752.

Reddy, J.N. (2007), "Nonlocal theories for bending, buckling and vibration of beams", *Int. J. Eng. Sci.*, **45**(2), 288-307.

Reddy, J.N. (2010), "Nonlocal nonlinear formulations for bending of classical and shear deformation theories of beams and plates", *Int. J. Eng. Sci.*, **48**(11), 1507-1518.

Reddy, J.N. (2011), "Microstructure-dependent couple stress theories of functionally graded beams", *J. Mech. Phys. Solids*, **59**(11), 2382-2399.

Reddy, J.N. and Pang, S.D. (2008), "Nonlocal continuum theories of beams for the analysis of carbon nanotubes", *J. Appl. Phys.*, **103**(2), 023511.

Ren, Q. and Tian, H. (2016), "Numerical solution of the static beam problem by Bernoulli collocation method", *Appl. Math. Model.*, **40**(21-22), 8886-8897.

Reutskiy, S.Y. (2017), "A new semi-analytical collocation method for solving multi-term fractional partial differential equations with time variable coefficients", *Appl. Math. Model.*, **45**, 238-254.

Rezaiee-Pajand, M. and Masoodi, A.R. (2018), "Exact natural frequencies and buckling load of functionally graded material tapered beam-columns considering semi-rigid connections", *J. Vib. Control*, **24**(9), 1787-1808.

Ru, C.Q. (2010), "Simple geometrical explanation of Gurtin-Murdoch model of surface elasticity with clarification of its related versions", *Sci. China Phys. Mech. Astron.*, **53**(3), 536-544.

Sekkal, M., Fahsi, B., Tounsi, A. and Mahmoud, S.R. (2017), "A novel and simple higher order shear deformation theory for stability and vibration of functionally graded sandwich plate", *Steel Compos. Struct, Int. J.*, **25**(4), 389-401.

She, G.L., Yuan, F.G., Ren, Y.R. and Xiao, W.S. (2017), "On buckling and postbuckling behavior of nanotubes", *Int. J. Eng. Sci.*, **121**, 130-142.

Shi, G. (2007), "A new simple third-order shear deformation theory of plates", *Int. J. Solids Struct.*, **44**(13), 4399-4417.

Şimşek, M. and Reddy, J.N. (2013), "Bending and vibration of functionally graded microbeams using a new higher order beam theory and the modified couple stress theory", *Int. J. Eng. Sci.*, **64**, 37-53.

Stamenković, M., Karličić, D., Goran, J. and Kozić, P. (2016), "Nonlocal forced vibration of a double single-walled carbon nanotube system under the influence of an axial magnetic field", *J. Mech. Mater. Struct.*, **11**(3), 279-307.

Tahouneh, V. (2017), "Vibration and mode shape analysis of sandwich panel with MWCNTs FG-reinforcement core", *Steel Compos. Struct, Int. J.*, **25**(3), 347-360.

Thai, H-T. and Vo, T.P. (2012a), "Bending and free vibration of functionally graded beams using various higher-order shear deformation beam theories", *Int. J. Mech. Sci.*, **62**(1), 57-66.

Thai, H-T. and Vo, T.P. (2012b), "A nonlocal sinusoidal shear deformation beam theory with application to bending, buckling, and vibration of nanobeams", *Int. J. Eng. Sci.*, **54**, 58-66.

Toghroli, A., Darvishmoghaddam, E., Zandi, Y., Parvan, M., Safa, M., Abdullahi, M.M., Heydari, A., Wakil, K., Gebreel, A.M.S. and Khorami, M. (2018), "Evaluation of the parameters affecting the Schmidt rebound hammer reading using ANFIS method", *Comput. Concrete, Int. J.*, **21**(5), 525-530.

Touratier, M. (1991), "An efficient standard plate theory", *Int. J.*

Eng. Sci., **29**(8), 901-916.
Wattanasakulpong, N. and Mao, Q. (2015), "Dynamic response of Timoshenko functionally graded beams with classical and non-classical boundary conditions using Chebyshev collocation method", *Compos. Struct.*, **119**, 346-354.
Zhou, J.K. (1986), "Differential Transformation and its Application for Electrical Circuits".

CC